Nonexponentialities in the Ultrafast Electron-Transfer Dynamics in the System Oxazine 1 in *N*,*N*-Dimethylaniline

S. Engleitner, M. Seel, and W. Zinth*

Institut für Medizinische Optik, Ludwig-Maximilians-Universität München, Oettingenstrasse 67, 80538 Munich, Germany

Received: November 10, 1998; In Final Form: February 18, 1999

Transient absorption experiments with probing in the blue part of the spectrum (440−500 nm) are performed for the electron-transfer system oxazine 1 in *N*,*N*-dimethylaniline. The experiments with high time resolution of better than 20 fs show pronounced modulations due to high-frequency wave packet motion (600 cm^{-1}) in the excited electronic state of the oxazine 1 molecule before electron transfer. Additionally, modulations due to wave packet motion in the product state of oxazine 1 after complete charge separation are observed. The absorption transients related to the electron transfer from *N*,*N*-dimethylaniline to oxazine 1 are clearly nonmonoexponential with time constants of 30 and 80 fs. This behavior points to a strong adiabaticity of the electron-transfer reaction with a high relevance of nuclear motions.

1. Introduction

Until recently, ultrafast photochemical reactions could only be studied indirectly. Quasistationary methods such as quantum efficiencies allowed the estimation of reaction rates. However, detailed information on the reaction dynamics was not accessible. In this context, qualitative and classical theories were widely used to describe the reactions. More elaborate models considering, e.g., the full quantum mechanical nature of the problem, the nuclear interactions with the vibrational relaxation, and the interaction with the solvent could not be checked by experiments. The recent development of ultrafast spectroscopy with the possibility of triggering a chemical reaction with a light pulse of a few femtoseconds duration and the subsequent study of transient absorption features with similar temporal resolution now supplies detailed information on fast reaction dynamics: (i) oscillatory absorption and emission dynamics due to wave packet-like excitation of vibrational modes in the excited electronic state were found,[1−10] (ii) stepwise formation of a reaction product related to the vibrational motion in the reactant was recorded for the one-dimensional photodissociation in NaI,[11] (iii) strong nonexponentialities were observed in ultrafast electron-transfer reactions pointing to the importance of nuclear motions for the electron transfer.[12]

The high temporal resolution available in the experiments stimulated the direct comparison with theoretical simulations. Realistic ab initio calculations were performed for reactive systems with several relevant nuclear degrees of freedom and with the explicit treatment of the ultrafast optical pump−probe experiment.[13]

It is the purpose of the present paper to supplement the known experimental data on the system oxazine 1 in *N*,*N*-dimethylaniline[14,15,16] with experimental data taken in the spectral range of electron-transfer product absorption (blue part of the spectrum) with highest temporal resolution. The experiments show convincingly the nonexponentiality of the initial reaction and vibrational wave packet motion in the reaction products. In addition, we present a global analysis of experimental data performed in the blue and red spectral range which allows characterization of the various reaction intermediates.

2. The System Oxazine 1 in *N*,*N*-Dimethylaniline

In a number of publications the system oxazine 1 ($OX1^+$) dissolved in *N*,*N*-dimethylaniline (DMA) has proven to be an ideal candidate for the study of extremely fast electron-transfer processes.[14−18] It has been shown that $OX1^+$ and DMA form weakly bound complexes[17] where optical excitation of the $OX1^+$ molecule triggers the electron transfer from the donor DMA to the acceptor $OX1^+$. This reaction to the charge-separated state (CSS) occurs faster than 100 fs. The first qualitative modeling of the initial absorption dynamics showed that the decay of the excited electronic state contains a process with a time constant of about 80 fs. An additional earlier absorption transient points to the existence of an even faster initial reaction component on the time scale of 30 fs.[16] In a very recent paper, nonexponential decays were found when the fluorescence emission of $OX1^+$ in DMA was recorded with the high temporal resolution of 70 fs.[18] This paper showed a dominant 60 fs component at short wavelengths (680 nm, close to the peak of the fluorescence emission, and 733 nm). Slower components were observed at weak amplitudes and in the long-wavelength wing of the emission spectrum. The authors assigned this nonexponentiality to different configurations of the electron-transfer partners leading both to a spectral shift of the emission and to a slow electron transfer. The observed amplitudes and the wavelength dependence suggest that only a minor fraction of the molecules has disturbed surroundings and undergoes slow electron transfer.

More detailed experimental data for the ultrafast forward electron transfer from DMA to $OX1^+$ obtained from time-resolved absorption experiments will be presented below in Figure 5. The backreactions following the initial electron transfer are considerably slower. From the charge-separated state (CSS, see Figure 1a) $OX1^{\bullet}/DMA^+$, the system reacts back to the electronic ground state of the reactants in approximately 3−4 ps. Since the complete dissipation of excess energy to the surroundings is not possible within this short time, higher vibrational levels are populated in the electronic ground state. The cooling of this hot ground state (HGS) occurs in the 7 ps regime. When replacing the strong electron donor DMA by another solvent like 1-chloronaphthaline (1CN), no electron

10.1021/jp9843712 CCC: $18.00
Published on Web 04/03/1999

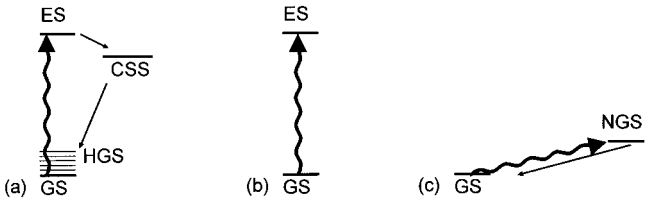

Figure 1. Reaction scheme for the electron-transfer cycle of the reactive system $OX1^+$ in DMA (a) and the nonreactive reference system $OX1^+$ in 1CN (b). Impulsive Raman scattering of the pump pulse leads to the nonstationary ground-state NGS (c). This reaction is found in both the reactive and the nonreactive system. Assignment of states: GS = ground state, ES = excited state, CSS = charge-separated state, HGS = hot ground state, NGS = nonstationary ground state.

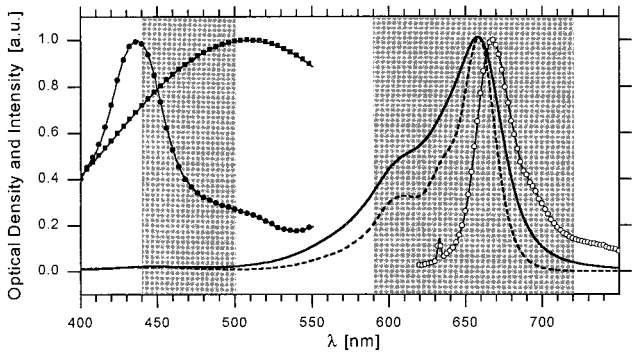

Figure 2. CW-absorption spectra of $OX1^+$ in DMA (—) and $OX1^+$ in 1CN (- - -). The absorption spectra of $OX1^\bullet$ (●) and DMA^+ (■) were obtained by reduction/oxidation of the educts $OX1^+$ and DMA at room temperature. The fluorescence spectrum of $OX1^+$ in 1CN is shown by open circles. All spectra are normalized. The spectral range covered by the time-resolved experiments is shown by a gray background.

transfer occurs, which results in the rather long lifetime (almost infinite on the observed time scale) of the excited electronic state S_1 of $OX1^+$ (ES). The optical properties of the different molecules studied in this paper are summarized in Figure 2. $OX1^+$ in 1CN has an absorption peak due to the $S_0 \rightarrow S_1$ transition at 657 nm (broken curve). The fluorescence emission spectrum peaks at 670 nm (open circles). The maximum of the absorption spectrum of $OX1^+$ in DMA (solid curve) is again located at 657 nm. This absorption spectrum is considerably broader than that of $OX1^+$ in 1CN. This may be due to the interaction between $OX1^+$ and the solvent DMA. The fluorescence emission of $OX1^+$ in DMA is strongly quenched and cannot be recorded by standard equipment. This points to a very rapid decay of the excited electronic state as it is found in the time-resolved experiments. When recording the resonance Raman spectrum, the fluorescence background was found to have its maximum at 675 nm with a half-width of roughly 50 nm. (Due to the high concentration of the sample used in the Raman experiment, a red shift of the recorded band due to reabsorption cannot be excluded.) The large spectral width of the emission spectrum may be taken as an indication for a rapid depletion of the excited electronic state of $OX1^+$. Since only small changes of the absorption peak position of $OX1^+$ in 1CN are found relative to $OX1^+$ in DMA (besides the changed width of the absorption band), $OX1^+$ in 1CN is used as a nonreactive reference system in the time-resolved experiments.

In vitro room-temperature preparations of the products of the electron-transfer reaction absorb in the blue part of the spectrum. When $OX1^+$ is reduced to $OX1^\bullet$ by means of tetrathiafulvalene (solvent methanol), it shows a maximum in the absorption spectrum at 437 nm (filled circles in Figure 2). The oxidized form DMA^+ prepared by adding *p*-benzoquinone has a very

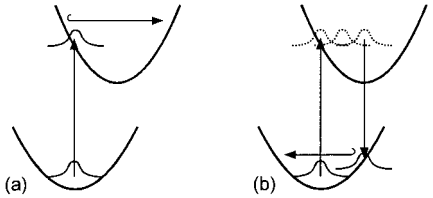

Figure 3. Schematic view of the generation of excited-state (a) and ground-state (b) wave packet by the pump pulse.

broad absorption band with a maximum around 505 nm (squares in Figure 2).

When a light pulse with a duration shorter than the period of the vibrational mode (which is coupled to the electronic transition) is absorbed in a molecule, it generates a superposition of vibrational levels in the excited electronic state (S_1 wave packet, see Figure 3a) which oscillates on the S_1 surface with the frequency ν of the vibrational mode. During this vibration it modulates the transitions out of the S_1 state and leads to oscillatory features in transient absorption experiments. Qualitatively, the wavelength dependence of the oscillation amplitude is related to the slope of the spectrum originating from the S_1 state. This means that the oscillation amplitude is determined by the excited-state absorption and stimulated emission spectrum. When the exciting pulse is long enough it interacts with the evolving wave packet and projects the excitation back to the electronic ground state. In this way, a nonequilibrated ground state (NGS, see Figure 1c) is formed with a vibrational excitation in the form of an S_0 wave packet (Figure 3b). The features related to the ground-state wave packet motion have a spectral dependence connected to the slope of the absorption spectrum originating from state NGS, which should be similar to the CW-absorption spectrum. Both kinds of wave packet motions are observed in the $OX1^+$ sample in the red spectral part.[16]

Optical excitation of the $OX1^+$ molecule at 630 nm produces oscillatory absorption changes pointing to wave packet motions with frequencies in the 600 cm^{-1} range. For the reactive system $OX1^+$ in DMA there is a S_1 wave packet motion which is quickly damped with the time constant of the electron-transfer reaction.[16] Only ground-state wave packet motion is seen later on. The wave packet motion was found to extend to several picoseconds in the nonreactive system. The wave packets are composed of at least two modes which are also seen in the resonance Raman spectrum at 567 and 608 cm^{-1} (see Figure 4). In the resonance Raman spectrum of $OX1^+$ in DMA, a number of vibrational modes at higher frequencies are also present. However, no pronounced low-frequency mode was observed in the range 200−560 cm^{-1}. In pure DMA (see Figure 4, bottom) there are several Raman-active modes around 1000 and 740 cm^{-1}. In the 600 cm^{-1} regime, where the wave packet motion occurs in the $OX1^+$ in the DMA system, only a weak band at 617 cm^{-1} is found.

When the absorption changes are recorded in the blue spectral range, more detailed information on the electron-transfer reaction is expected. The absorption band of the product should allow one to find the changes due to the formation and decay of the excited electronic state OX1* and the formation of the reaction products $OX1^\bullet$ and DMA^+.

3. Materials and Methods

3.1. Experimental Setup. A colliding pulse mode-locked (CPM) dye laser, pumped by a CW argon-ion laser, was used to generate pulses at 630 nm with a duration (fwhm) of about 50 fs and 0.2 nJ pulse energy. These pulses were amplified at

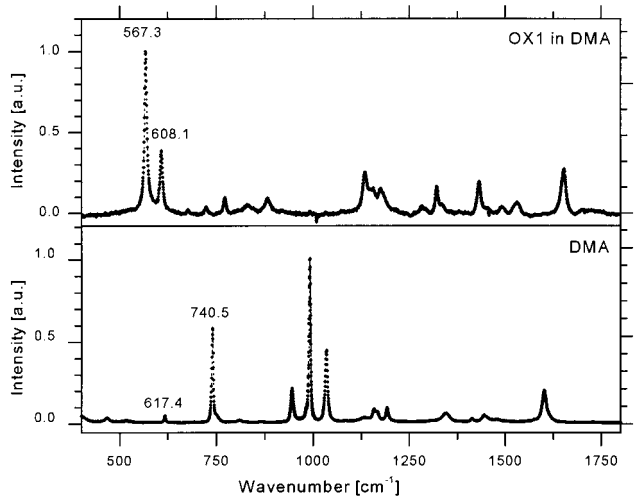

Figure 4. Resonance Raman spectrum of $OX1^+$ in DMA (upper part), and Raman spectrum of pure DMA (lower part). Excitation wavelength = 632.8 nm.

a 10 Hz repetition rate in a multipass dye amplifier, pumped by the second harmonic of a Q-switched Nd:YAG laser. After recompression, pulses with an energy of 15 μJ and a duration of about 50 fs at a center wavelength of 630 nm were available. The beam was now split in two parts by a quartz wedge. The excitation part and the probing part for the one-color (red/red) experiments were used directly after fiber compression. In the two-color (red/blue) experiments, the split part was used for continuum generation in a sapphire plate. The continuum was selectively amplified in another multipass dye amplifier giving pulses with a center wavelength of 465 nm and a duration of about 50 fs after recompression.

Both pump and probe pulses were further compressed in a fiber-grating prism compressor.[19] Compression to 9 fs at a center wavelength of 630 nm and to 14 fs at a center wavelength of 465 nm was achieved. After the final compression stage, the probing part was split again into the actual probing and a reference part.

The geometry of the sample-setup itself was optimized for highest time resolution. Spherical mirrors were used for focusing pump, probe, and reference beams to the sample. The sample was contained in a quartz flow cell with a 10 μm path length.

The time resolution was controlled by measuring the cross-correlation between pump and probe pulses at the location of the sample cell by a 50 μm thick KDP crystal. The width (fwhm) of the cross-correlation function was 15 fs for the one-color and 18 fs for the two-color experiments.

Behind the sample, the probe and reference beam were dispersed in two 0.25 m monochromators and imaged on photodiode arrays. The wavelength resolution (6 nm for one-color and 2 nm for two-color experiments) was adapted to the spectral range and to the time constants of the observed processes.

The one-color experiments covered the spectral range between 585 and 720 nm and the two-color experiments between 440 and 510 nm.

3.2. Sample Preparation. Oxazine 1, obtained from Lambda Physik (LC7250), *N*,*N*-dimethylaniline (CAS−Nr. 121−69−7), and 1-chloronaphthaline (CAS−Nr. 90−13−1), both obtained from Merck, were used without further purification. To get a significant optical density of the sample (path length 10 μm), OX1 concentrations of about 10^{-2} M had to be used. To achieve such high concentrations in the solvents DMA and 1CN, the following procedure was used: OX1 was first dissolved in a small amount of methanol. This concentrate was added to DMA and 1CN, respectively. The resulting mixture contained less than 5% vol of methanol. The methanol concentration was further reduced by evaporation. Residual methanol impurities should not interfere with the initial electron-transfer process.[17] No indications (e.g., changes of the absorption spectrum) for aggregation could be found. The optical density of the sample with a path length of 10 μm was about 1.5.

3.3. Data Modeling: General Remarks. Information on the kinetics of electron transfer is contained in the depopulation dynamics of the excited state and the dynamics of formation of the electron-transfer products. The corresponding S_1 processes, stimulated emission, and excited-state absorption are mixed with the ground-state bleach and stimulated Raman contributions to give the overall transient transmission signal. Therefore, careful modeling is necessary to disentangle this mixture and to extract the kinetics of electron -transfer. There are different approaches: Detailed quantum mechanical modeling is very tedious (if not impossible) for big or even medium-sized molecules. For that reason, in many cases a phenomenological approach is used: The population dynamics are modeled by a system of rate equations leading to (multi-) exponential decays of the transient transmission. The method relies on thermal equilibration of the nonelectronic degrees of freedom of the molecular system under investigation. This is clearly not the case for electron transfer on the 100 fs time scale.

The simulation of the modulations caused by vibrational wave packet motion can be done by a superposition of sinusoidal functions with individual amplitudes and phases for each involved mode at each observation wavelength. For dispersed data acquisition, this concept leads to a tremendous amount of parameters without physical connections. Optimization of the set of parameters in a conventional nonlinear least-squares algorithm shows a strong mixing of various subgroups of the parameters, because of model inabilities and measurement error. As a consequence, the resulting amplitude spectra tend to show a very high error.

In the data handling of this paper we used another approach: A close look at experimental[16] and simulated[20,21] data shows that to a first approximation wave packet motion only leads to a spectral shift of the affected absorption or emission processes. Exploiting this observation, the use of harmonically shifted spectra to construct the modeling function has two advantages: First, the number of free parameters can be reduced significantly by taking advantage of the inherent spectral smoothness of the involved spectra. The phase of the modulation (ϕ_j) and the spectral shift (λ_j) are now parameters coupled to the wave packet motion (not to individual observation wavelengths), further reducing the number of parameters. Second, the higher harmonics of the fundamental beat frequency ω_j, which are observed in the experimental data, are automatically included, thus avoiding the crude approximation of only one sinusoidal wave per mode. The resulting fitting function for the transient transmission change $\Delta T/T$ measured as a function of wavelength λ and delay time Δt has, therefore, the structure:

$$\frac{\Delta T}{T}(\lambda,\Delta t) = \sum_i a_i(\Delta t) S_i(\lambda,\Delta t) = \sum_i a_i(\Delta t) S_i\left(\lambda - \sum_j \hat{\lambda}_j \sin(\omega_j \Delta t + \phi_j)\right) \quad (1)$$

The $a_i(\Delta t)$ values are the weight factors of the spectra for the different processes (ground state bleach, stimulated emission, etc.). They carry information on the population dynamics of

the various states and consist of superpositions of exponential decays. These correspond to the rate equation system for the population of molecules undergoing electron transfer but also for molecules staying in the electronic ground state after Raman interaction with the pump pulse. The spectral variation of the transient transmission $\Delta T/T$ is fully contained in the spectral shape of the various S_i. The delay time (Δt) dependent part only shows up for processes modulated by wave packet motion (e.g., stimulated emission), summing up the contributions of the involved vibrational modes (index j). Additionally, the model function can easily be extended to include dynamic solvent effects (spectral shifts). Within this concept it should be much easier to construct a phenomenological but consistent model represented by a relatively small set of parameters.

3.4. Data Modeling: Details. On the basis of the results of previous experiments,[16] the reaction scheme depicted in Figure 1 was established. Excitation by the pump pulse leaves a fraction q of the molecules (see Figure 1a) in the excited electronic state ES which is quickly depleted by electron transfer (time constant is less than 100 fs). The charge-separated state (CSS) lives for a few picoseconds before the system returns to a vibrationally excited ("hot") ground-state HGS. The subsequent cooling proceeds on the 7 ps time scale. The whole electron-transfer and relaxation cycle is completed in about 10 ps.[15,16] The remaining $1 - q$ molecules (see Figure 1c) undergo a stimulated Raman interaction with the pump pulse, leading to a vibrational wave packet moving on the potential surface of the electronic ground-state NGS.[21,22] In the one-color experiments, ground-state depletion, stimulated emission, and excited-state absorption can be observed for the molecules in the electron-transfer cycle. Some of these processes carry information on the electron-transfer kinetics. Thus, they have to be separated from the contributions emerging from the nonstationary ground-state NGS built up by the stimulated Raman process. In the two-color experiments, no contributions of the nonstationary ground state are observed (see below). In this case, the transient transmission is a superposition of ground-state bleach, stimulated emission, excited-state absorption, and product absorption.

The processes for both experiments are modulated by a superposition of two vibrational wave packets corresponding to the vibrational modes observed at 657 and 608 cm^{-1} in the resonance Raman spectrum (see Figure 4). Because of the very high speed of the initial electron transfer, the population decay of the excited state and the build-up of the electron-transfer products cannot be modeled by a superposition of exponential decays (i.e., by rate equations). Thus, the weight factors $a_i(t)$ for the excited-state processes cannot be included in the model functions for the reactive system. Accordingly, data at short delay times, up to 200 fs, is not used for fitting and the corresponding spectra are missing in Figure 7 for the reactive system.

The nonreactive reference system OX1 in 1CN was modeled in an analogous way (compare reaction scheme Figure 1b and Figure 1c). Due to the almost infinite (in relation to the time scale of observation) lifetime of the excited state in the nonreactive system, there is no restriction on the modeling of the excited-state processes.

To achieve maximum flexibility, all the spectra were modeled by cubic splines. The number of fixed points for the splines was roughly one-third of the number of observation wavelengths.

4. Results

Experimental data on $OX1^+$ in DMA recorded in the blue spectral range are shown in Figure 5. In the upper part, the data

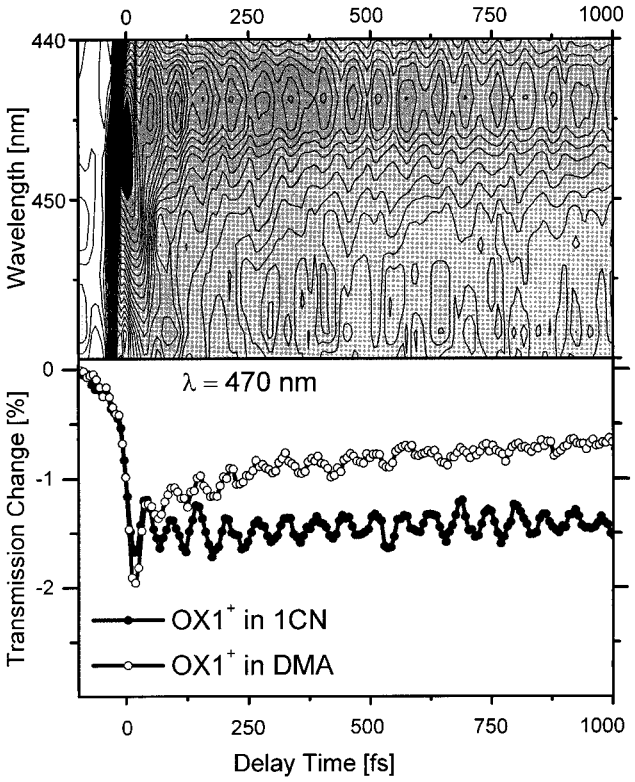

Figure 5. Transient transmission spectra of the reactive system $OX1^+$ in DMA between 440 and 458 nm (upper part) and for both reactive (○) and nonreactive system (●) (lower part). The curves in the lower part are not normalized, thus giving slightly different absorption maxima for reactive and nonreactive systems due to different absorption cross sections and sample preparations.

for recording wavelengths 440−458 nm and delay times up to 1000 fs are shown in a 2-D contour plot, where dark colors are used for strong absorption increases while white indicates weak changes. The overall features are seen well in this plot. At time zero there is a strong absorption increase, decaying later on very quickly. There is an oscillatory structure superimposed on this initial decay. After about 200 fs the transient features change: the decay becomes much slower and pronounced oscillations are still seen. The absorption changes are strongest at short wavelengths around 445 nm. In the lower part of Figure 5, the absorption transients for $\lambda = 470$ nm are recorded for the reactive (open circles) and the nonreactive system (filled circles). The early time dependence is as follows: The nonreactive $OX1^+$ in 1CN shows a strong initial absorption increase (transmission decrease) around zero delay time. Subsequently, one finds pronounced oscillations while the average absorption change stays almost constant during the first 500 fs. This can be seen in Figure 6, where the time dependence is plotted for the spectrally integrated signal for long delay times. During the first 20 ps one finds only a very weak decrease of the transmission change for the nonreactive system. The data support the observations in the red spectral range. The observed transmission decrease indicates that the absorption of the excited electronic state of $OX1^+$ in the blue spectral part (450−500 nm) is stronger than the absorption of the ground state of $OX1^+$. From the analysis of the spectrally resolved signal, the absorption spectrum of the S_1 state is calculated and shown in Figure 7, upper left part (open circles).

The modulation of the absorption change has a period of approximately 55 fs. The improved analysis of the data of the red spectral part (see below) allows one to extract the relative contribution of S_1 and S_0 wave packets to the observed

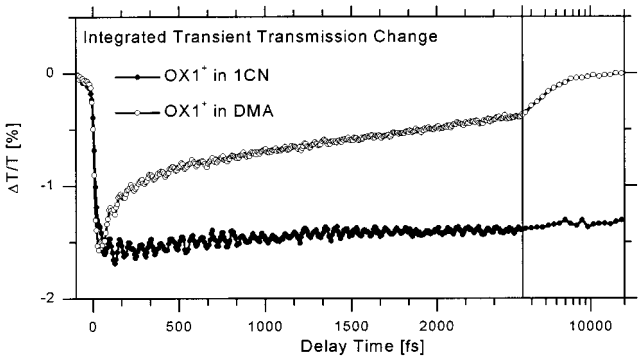

Figure 6. Spectrally averaged transient transmission change on the long time scale. The probing light transmitted through the sample was averaged over all detectors, i.e., from $\lambda = 441$ to 500 nm.

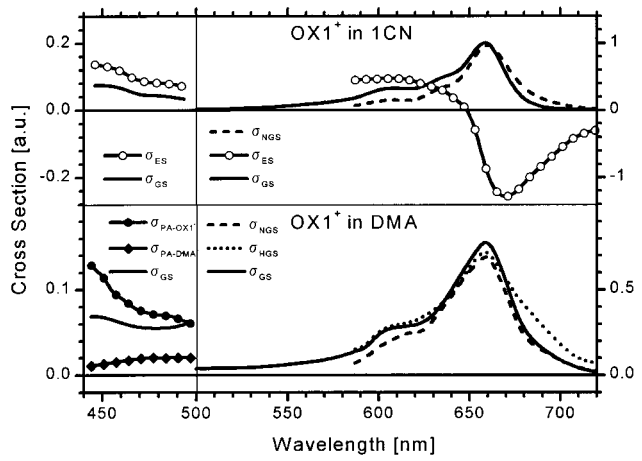

Figure 7. Spectra for transient states calculated by the model described in Materials and Methods. Excited-state contributions are marked with open symbols, while product-state contributions are shown with filled symbols. Ground-state contributions are shown with lines only (see text). Since ultrafast components below 100 fs are not covered by the presented model, the excited-state contributions for the reactive system (lower part) are not shown.

modulations. The analysis shows that the modulations are predominantly due to the S_1 wave packet motion. The S_0 wave packet is prepared at lower vibrational levels and correspondingly with a much weaker amplitude. In addition, the smooth slope of the ground-state absorption spectrum in the blue spectral range leads to much weaker absorption modulations.

The time dependence found for $OX1^+$ in DMA (open circles in Figures 5 and 6) is more complicated. After the initial transmission decrease due to excited-state absorption of OX1*, a strongly modulated transmission increase is found upon formation of the charge-separated state (Figure 5 lower part, open circles). After 250 fs, the population of the excited state has vanished due to electron transfer from DMA to $OX1^+$ and the average absorption change has become much weaker. The transmission decrease found in this time range is related to increased absorption from the OX1• and the DMA^+ radicals. This net absorption increase found in the blue spectral range for long delay times shows that the absorption of the electron-transfer products OX1• and the DMA^+ overcompensates the absorption decrease, which is expected from bleaching of the (weak) ground-state absorption in this spectral range. The transmission change decays with a time constant of about 3 ps (see Figure 6, open circles). This process is related to the back transfer of the electron to the DMA. The hot ground state reached in this way decays with a time constant of approximately 6 ps. This process does not lead to absorption

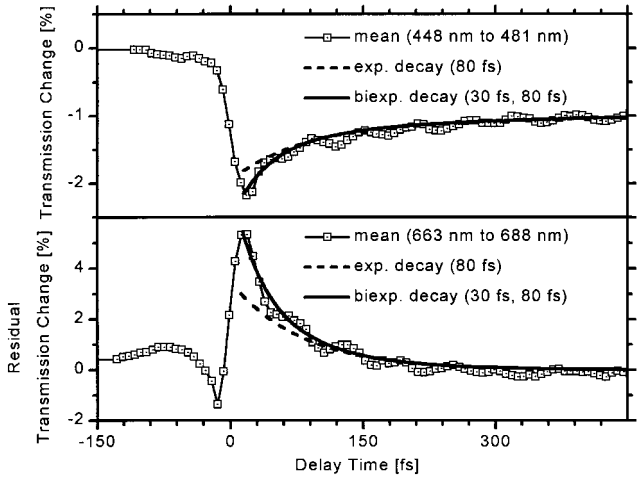

Figure 8. Spectrally averaged transient transmission change recorded in the blue spectral range (upper part) and averaged residual (see text) transmission change in the red spectral range (lower part) showing the nonmonoexponentiality of the decay due to electron transfer. Only a biexponential fitting function (—) is able to give a qualitative description of the initial reaction. The signal at and before zero delay time is influenced by coherent artifacts and cross-phase modulation between pump and probe pulses.

changes in the blue spectral range. The lack of transmission changes for very late delay times indicates that there is no long-lasting S_1 state generated by the optical excitation process.

Surprisingly, the modulated absorption is found not only during the population of the excited electronic state, but also at delay times up to about 1000 fs when electron transfer is already completed. These oscillations have the same relative phase as the oscillations observed in the excited electronic state of the nonreactive system. A straightforward interpretation relates this oscillation to a wave packet motion of the OX1• radical, which has survived the electron-transfer step.

The details of the very early time dependence of the transmission change can be deduced from Figure 8, upper part, where the transmission changes are averaged over the spectral range from 448 to 481 nm. This average signal still shows the oscillations due to wave packet motion. They are superimposed on a very rapid initial recovery of the transmission followed by a slower process. Averaging over the oscillations allows the simulation of the kinetics of the transfer process: One finds that a monoexponential decay is unable to explain the data. A pure 80 fs process (broken curve) can fit the later absorption changes. However, such a process does not fit the kinetics during the first 50 fs. Only a biexponential model function with the use of a short decay time (about 30 fs) allows a qualitative match.

A similar behavior is found for the red spectral range. Since the long-lasting absorption changes due to the bleaching of the ground-state absorption are strong and superimposed on the earlier transients, the fast time dependence was extracted in a more elaborate procedure. The slower kinetics caused by the back-electron transfer and the modulations due to S_0 wave packet motion were fitted based on the data taken at later delay times. Subsequently, they were subtracted from the experimental data. Averaging the residual absorption changes from 668 to 688 nm leads to the curve of Figure 8, lower part. The feature before time zero is due to a coherent artifact related to the high spectral resolution of the detection system.[24] For positive delay times, where the signal is undisturbed, we find again a strong nonmonoexponential decay, which can be fitted by the time constants and the same amplitude ratio used before in the blue

spectral range. The data indicates that the decay of the excited electronic state OX1* and the formation of the charge-separated state is biphasic with a fast 30 fs and a slower 80 fs component.

The data handling procedure given in Materials and Methods (section 3) allows a new evaluation of the data taken in the red spectral range, giving access to the different intermediate states of the reaction process. The absorption spectra for the different states are plotted in Figure 7. The solid curve gives the ground-state absorption σ_{GS} recorded directly with a CW spectrometer: Optical excitation promotes the system to state OX1* (σ_{ES}), represented by the open circles. The properties of this state can be obtained for the nonreactive system. It contains contributions from excited-state absorption (at shorter wavelengths) and stimulated emission. For the reactive system $OX1^+$ in DMA, the short lifetime of OX1* imposes additional uncertainties: The short lifetime and the complicated decay kinetics do not allow a convincing modeling of the excited-state contribution. Therefore, the excited-state absorption/emission spectrum is not shown in Figure 7 for the reactive system. The nonequilibrated ground-state NGS which is related to the S_0 wave packet motion is shown by the dashed curves (σ_{NGS}). The spectrum shows a slight red shift, relative to the CW spectrum of the ground state (σ_{GS}). The analysis shows that the ground-state wave packet is prepared with an amplitude which is approximately 4 times smaller than the amplitude of the S_1 wave packet. Therefore, it is seen well only in spectral ranges with a strong slope of the spectrum of state NGS. The dotted curve gives the absorption spectrum of the hot ground state σ_{HGS} which is formed after completion of the back-electron transfer. In this state, most of the energy of the exciting photon (2 eV) is transferred to vibrational excitation, heating the oxazine molecule. The resulting spectrum shows the features expected for such a hot molecule: The spectrum is strongly broadened and there is a pronounced increase of the red wing of the absorption spectrum.

In the spectral range around 600 nm, the absorption change due to the charge-separated state (CSS) is dominated by the absorption bleach of the $OX1^+$ absorption band. Possible contributions due to the products $OX1^\bullet$ and DMA^+ cannot be identified. However, the $OX1^\bullet$ product absorption becomes clearly visible in the blue spectral range. The filled circles in Figure 7 represent the absorption spectrum related to $OX1^\bullet$. The observed spectrum qualitatively follows the CW-absorption data of $OX1^\bullet$ presented in Figure 2. Only a weak contribution from DMA^+ is required for the fitting of the experimental data. This points to a small absorption cross-section of the radical cation DMA^+ in this spectral range.

The direct experimental results on the fast electron-transfer reaction in OX1 can be summarized as follows: (i) There is a pronounced wave packet motion in the S_1 state, the S_0 state, and in the reaction product $OX1^\bullet$. (ii) The electron-transfer kinetics are not monoexponential. There is a fast initial reaction step with a time constant of about 30 fs and a subsequent slower process with a time constant of about 80 fs. (iii) The spectra of the intermediates are consistent with the reaction model presented in Figure 1.

5. Discussion

5.1. Wave Packet Motion in the Reaction Product. The observation of oscillatory absorption changes extending to delay times where the excited-state species OX1* has already vanished due to electron transfer from DMA to $OX1^+$ strongly supports the interpretation that the observed vibrational wave packet is localized in the product state. A connection to the DMA^+ radical can be ruled out since the DMA^+ radical has a much weaker absorption and a smoother wavelength dependence than $OX1^\bullet$. The coincidence of the observed modulation frequency with the vibrational frequency of $OX1^+$ indicates that the wave packet-like excitation is localized on the $OX1^\bullet$ radical. No phase difference between the modulations in the reactive and nonreactive system, i.e., between the wave packet motion in the excited state and the charge-separated state, is found. The experimental observations indicate that the vibrational frequency does not change considerably upon reduction of the $OX1^+$ molecule. This supplements the finding that the vibrational frequencies of the S_0 and S_1 wave packet motion are very similar (see above) and indicates that the frequencies of the observed modes do not depend strongly on excitation or transfer of an electron. The coupling of nuclear motion and electron transfer seems to result predominantly in a shift of the equilibrium position of the vibrational mode in the different states. Two special arrangements of the potential-energy surfaces which are consistent with the phases of the modulations caused by the various wave packets are shown in Figure 9 and are discussed below.

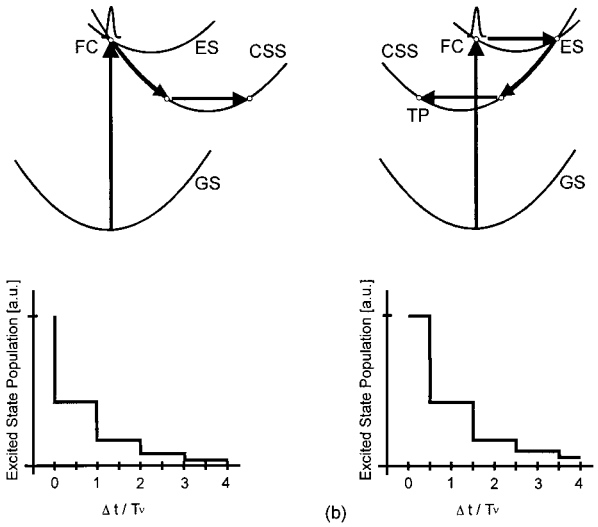

Figure 9. Upper part: Schematic view of potential-energy surfaces and wave packet motion for the possible arrangements consistent with the observed phases of the modulation of the transient transmission. Lower part: Qualitative view of the decay of the excited-state population resulting from the two possible arrangements deduced from a simplified reaction model. The experimental data suggest that the model presented at the right side should be realized in the electron transfer from DMA to $OX1^+$.

5.2. Nonexponentiality of the Initial Electron Transfer. Both sets of data (from the red and the blue probing wavelengths) yield the early time dependence of the absorption to be nonmonoexponential with an ultrafast component (30 fs) and a slower one (80 fs) and superimposed oscillations (see Figure 8). Such a time dependence can be explained by qualitative arguments as well as by more explicit theoretical simulations where several modes are considered. Qualitatively a strong electronic coupling between the electron-transferring molecules leads to a high reaction probability each time the molecules reach the interaction region (adiabatic behavior). In a first-order approximation, the reaction is stepwise. More explicit theoretical considerations[22,23] suggest a situation with nonexponential reaction dynamics with a fast component of the electron transfer prior to the onset of dissipation, reflecting the vibrational motion. The following slower component would account for electron transfer with dissipation. An alternative interpretation could assign the nonexponentiality to different configurations of donor

and acceptor molecules. However, the strong wavelength dependence of the decay of the excited electronic state (and the electron transfer) found in ref 18 and our observation that the 30 and 80 fs components occur over a broad spectral range suggest that structural heterogeneities should not dominate the initial kinetics.

The electron-transfer kinetics for the proposed relative positions of the electronic potential-energy surfaces are depicted in a highly schematic way in the lower part of Figure 9. In this model we assume that the observed high-frequency wave packet moves on the reaction coordinate. This interpretation is reasonable but cannot be proven with the present experimental data. For case A, preparation of the wave packet by the optical excitation process leads to a Franck−Condon region which is also the region of transition to the charge-separated state. In this situation the population of the excited electronic state drops immediately at delay-time zero. Subsequent population decays occur separated by the period τ_{vib} of the S_1 wave packet mode(s). If the interaction region between the excited-state potential surface and charge-separated state is at the outer turning point of the S_1 vibrational motion (case B), the system stays for one-half a vibrational period in the excited electronic state before a first efficient electron-transfer step takes place. In both cases, a modulation of the population results. The observed time dependence with a fast but not instantaneous decay (time constant of about 30 fs, corresponding to approximately one-half a vibrational period) at early times supports the idea that the potential surfaces are arranged according to model B. On the contrary, case A should exhibit an initial drop of the transient transmission with a width corresponding to the width τ_{cc} of the cross-correlation function between pump and probe pulses, which is with $\tau_{cc} \approx 18$ fs, significantly faster than the observed behavior.

However, the observed modulation in the reactive system cannot be assigned to a stepwise electron-transfer alone: The absorption changes due to S_1 wave packet motion are superimposed on the electron-transfer kinetics. More explicit[23] simulations using a multidimensional potential surface indicate that only weak population modulations combined with a biphasic time dependence should result from electron transfer: The first fast reaction part can be assigned to the adiabatic reaction with one relevant nuclear degree of freedom, while the set-in of relaxation and the coupling to other modes and a thermal bath decelerates the further reaction speed, giving the slower part of the observed biphasic decay.

In conclusion, we have seen from time-resolved experiments with the highest temporal resolution performed in the blue and red spectral range that vibrational motions play an important role in the ultrafast electron transfer in the system oxazine 1 in *N*,*N*-dimethylaniline. One observes strong high-frequency wave packet motion, not only in the originally prepared excited electronic state, but also in the reaction products after electron transfer. In addition, the nonmonoexponentiality of the absorption changes, related to the electron-transfer reaction, shows that the electron-transfer proceeds in the adiabatic regime, where the initial nuclear motion limits the reaction speed.

Acknowledgment. The authors gratefully acknowledge many stimulating discussions and valuable contributions by G. Stock and W. Domcke. The authors also thank I. Hartl for supplying us with high-quality resonance Raman spectra of oxazine 1 in DMA and P.O.J. Scherer for calculation of the vibrational modes of oxazine 1.

References and Notes

(1) Wise, F. W.; Rosker, M. J.; Tang, C. L. *J. Chem. Phys.* **1987**, *86*, 2827.
(2) Pollard, W. T.; Fragnito, H. L.; Bigot, J.-Y.; Shank, C. V.; Mathies, R. A. *Chem. Phys. Lett.* **1990**, *168*, 239.
(3) Mokhtari, A.; Chebira, A.; Chesnoy, J. *J. Opt. Soc. Am.* **1990**, *B7*, 1551.
(4) Vos, M. H.; Lambry, J.-C.; Robles, St. J.; Youvan, D. C.; Breton, J.; Martin, J.-L. *Proc. Natl. Acad. Sci. U.S.A.* **1991**, *88*, 8885.
(5) Vos, M. H.; Rappaport, F.; Lambry, J.-C.; Breton, J.; Martin, J.-L. *Nature* **1993**, *363*, 320.
(6) Vos, M. H.; Jones, M. R.; Hunter, C. N.; Breton, J.; Lambry, J.-C.; Martin, J.-L. *Biochemistry* **1994**, *33*, 6750.
(7) Stanley, R. J.; Boxer, S. G. *J. Phys. Chem.* **1995**, 99, 859.
(8) Spörlein, S.; Zinth, W.; Wachtveitl, J. *J. Phys. Chem. B* **1998**, *102*, 7492.
(9) Bradforth, S. E.; Jimenez, R.; van Mourik, F.; van Grondelle, R.; Fleming, G. R. *J. Phys. Chem.* **1995**, *99*, 16179.
(10) Dunn, T. J.; Sweetser, J. N.; Walmsley, I. A. *Phys. Rev. Lett.* **1993**, *70*, 3388.
(11) Rose, T. S.; Rosker, M. J.; Zewail, A. H. *J. Chem. Phys.* **1988**, *88*, 6672.
(12) Wynne, K.; Reid, G. D.; Hochstrasser, R. M. *J. Chem. Phys.* **1996**, *105*, 2287.
(13) Wolfseder, B.; Seidner, L.; Stock, G.; Domcke, W. *Chem. Phys.* **1997**, *217*, 275.
(14) Yartsev, A.; Nagasawa, Y.; Douhal, A.; Yoshihara, K. *Chem. Phys. Lett.* **1993**, *207*, 546.
(15) Kandori, H.; Kemnitz, K.; Yoshihara, K. *J. Phys. Chem.* **1992**, *96*, 8042.
(16) Seel, M.; Engleitner, S.; Zinth, W. *Chem. Phys. Lett.* **1997**, *275*, 363.
(17) Schneider, S.; Stammler, W.; Bierl, R.; Jäger, W. *Chem. Phys. Lett.* **1994**, *219*, 433.
(18) Rubtsov, I. V.; Shirota, H.; Yoshihara, K. In *Ultrafast Phenomena XI*; Elsaesser, T., Fujimoto, J. G., Wiersma, D. A., Zinth, W., Eds.; Springer Series in Chemical Physics; Springer: New York, 1998; Vol. 63, pp 633.
(19) Fork, R. L.; Brito-Cruz, C. H.; Becker, P. C.; Shank, C. V. *Opt. Lett.* **1987**, *12*, 483.
(20) Stock, G.; Domcke, W. *Phys. Rev.* **1992**, *A45*, 3032.
(21) Pollard, W. T.; Mathies, R. A. *Annu. Rev. Phys. Chem.* **1992**, *43*, 497.
(22) Domcke, W.; Stock, G. *Adv. Chem. Phys.* **1997**, *100*, 1.
(23) Wolfseder, B.; Seidner, L.; Domcke, W.; Stock, G.; Seel, M.; Engleitner, S.; Zinth, W. *Chem. Phys.* **1998**, *233*, 323.
(24) Joffre, M.; Hulin, D.; Migus, A.; Antonetti, A.; Guillaume, C. B.; Pegyhambarian, N.; Lindberg, M.; Koch, S. W. *Opt. Lett.* **1988**, *13*, 276.